Silica nanoparticle dissolution rate controls the suppression of *Fusarium wilt* of watermelon (*Citrullus lanatus*)

Hyunho Kang,[†] *Wade Elmer,*[‡] *Yu Shen,*[%] *Nubia Zuverza-Mena,*[‡] *Chuanxin Ma,*[‡] *Pablo Botella,*[§] *Jason C. White,*[‡] *Christy L. Haynes*[†*]

[†]Center for Sustainable Nanotechnology, Department of Chemistry, University of Minnesota, 207 Pleasant Street S.E., Minneapolis, Minnesota 55455, United States

[‡]Center for Sustainable Nanotechnology, The Connecticut Agricultural Experiment Station, 123 Huntington Street, New Haven, Connecticut 06504, United States

[%]Center for Sustainable Nanotechnology, Department of Chemistry, University of Wisconsin, 1101 University Avenue, Madison Wisconsin 53706 USA

[§]Instituto de Tecnología Química, Universitat Politècnica de València-Consejo Superior de Investigaciones Científicas, Avenida de los Naranjos s/n, 46022 Valencia, Spain

*Corresponding Author: chaynes@umn.edu

KEYWORDS: Silica nanoparticles, watermelon, Fusarium wilt, hydrolysis, disease suppression,

SYNOPSIS: In this study, the engineered silica nanoparticles were prepared to possess the different dissolution behaviors, to investigate their effects on the sustainable crop protection against fungal disease.

ABSTRACT

Projected population increases over the next 30 years have elevated the need to develop novel agricultural technologies to dramatically increase crop yield, particularly under conditions of high pathogen pressure. In this study, silica nanoparticles (NPs) with tunable dissolution rates were synthesized and applied to watermelon (*Citrullus lanatus*) to enhance plant growth while mitigating development of the *Fusarium wilt* disease caused by *Fusarium oxysporum* f. sp. *niveum*. The hydrolysis rates of the silica particles were controlled by the degree of condensation of or the catalytic activity of aminosilane. The results demonstrate that the plants treated with fast dissolving NPs maintained or increased biomass whereas the particle-free plants had a 34% decrease in biomass. Further, a higher silicon concentration was measured in root parts when the plants were treated with fast dissolving NPs, indicating effective silicic acid delivery. In a follow-up field study over 2.5 months, the fast dissolving NP treatment enhanced fruit yield by 81.5% compared to untreated plants. These findings indicate that the colloidal behavior of designed nanoparticles can be critical to nanoparticle-plant interactions leading to disease suppression and plant health, as part of a novel strategy for nano-enabled agriculture.

38 **Introduction**

39 With a predicted global population of 10 billion by 2050, the need for innovative agricultural
40 production strategies is great. Meeting this increased food production demand will be confounded
41 by other factors, including decreasing water/arable land resources and global climate change.[1–3]
42 Among these negative factors, the infection by fungal pathogens is particularly problematic, with
43 pathogenic activity limiting the productivity of a wide range of species such as rice, wheat, maize,
44 and soybean. It has been estimated that a variety of pathogens can cause up to 70% production
45 yield losses of those major crops.[4] *Fusarium wilt* is a fungal disease caused by host-specific strains
46 of a soil-borne pathogen called *Fusarium oxysporum*; there are strains that infect hundreds of
47 plants of economic importance, including both crop and ornamental species.[5] For example,
48 *Fusarium wilt* of watermelon (*Citrullus lanatus*) is a severe disease caused by *F. oxysporum* f. sp.
49 *niveum* (FON); importantly, this pathogen has increased in both incidence and severity due to the
50 loss of fumigants as a management strategy and to the popularity of highly susceptible seedless
51 cultivars.[6] The development of novel and sustainable approaches to effectively manage FON and
52 related fungal diseases is urgently needed for watermelon and many other crops.[6]

53 Nano-enabled techniques have received significant attention as a potential tool to replace or
54 complement the conventional methods of fungicides, biological control, and rotations with non-
55 susceptible crops.[7] Nanomaterials have demonstrated increased nutrient delivery efficiency and an
56 enhanced triggering of pathogen defense systems in a number of plant-pathogen systems, and the
57 silicon-based nanomaterials have been a topic of recent interest.[8–12] The application of silicon-
58 based nanoparticles to plants has been shown to improve stress tolerance, resulting in enhanced
59 yield.[13–16] In fact, silicon is considered as a biostimulant by inducing resistance to abiotic stresses,
60 diseases, and pathogens.[17] The precise mechanism of action is unclear, although it is known that

61 silica can be deposited beneath the plant cuticle to form a cuticle-silica double layer. This enhanced
62 structural barrier can then mechanically impede penetration by insect pests and fungal pathogens,
63 essentially derailing the infection process.[18] Silica treatment can also modulate host defense
64 mechanisms, including increasing plant defensive enzyme activity, altering plant hormones related
65 to the disease defense signaling pathways, or facilitating antimicrobial compound synthesis within
66 plant cells.[19–21]

67 In spite of the agricultural applications of various nanomaterials, how the colloidal property
68 of the nanoparticles is related to their performance inside plants are very underexplored. One
69 advantage of using silica nanoparticles is that their hydrolysis rates can be tuned to vary their
70 dissolution behaviors. In this work, six different spherical silica nanoparticles were synthesized to
71 control intraplant delivery of silicic acid, and five of those were foliarly applied to watermelon
72 (*Citrullus lanatus)* to investigate the hypothesis that the fastest dissolving nanoparticle would have
73 the largest effect on fungal disease suppression (*Fusarium wilt*). Measured endpoints in the
74 greenhouse and field conditions include biomass/yield, disease progress, elemental/nutritional
75 content, and the gene expression levels of a number of plant defense and general metabolism-
76 related genes. This is among the first study to systematically investigate the effect of engineered
77 mesoporous silica nanoparticle dissolution behavior as a sustainable crop protection strategy.

78

79 **Experimental Methods**

80 *Synthesis of Spherical Silica Nanoparticles and Rapid Dissolution Particles* For the six types of
81 silica nanoparticles used in this work were synthesized using a reverse microemulsion method.[22]
82 The dissolution rate of the nanoparticles prepared only with tetraethyl orthosilicate (TEOS)
83 without any further modification was considered as the standard rate ($_{CTL}SiO_2$ particle), and the
84 other particles exhibited more or less rapid dissolution as a function of slight modifications or

85 additional treatments during synthesis. First, in an Erlenmeyer flask, 152 mL of cyclohexane, 36
86 mL of 1-hexanol and 38.52 g of Triton x-100 were added and mixed by stirring. Then, 9.6 mL of
87 water was added dropwise with continuous stirring, followed by 2 mL of TEOS added dropwise.
88 After an hour of stirring, 2 mL of concentrated NH_4OH (28 – 30%) was added. The solution was
89 stirred for 24 hours at room temperature. After 20 – 24 hours, ethanol was added to break the
90 microemulsion, and the suspension was then centrifuged for 20 minutes at 65,400 relative
91 centrifugal force (RCF) to obtain silica pellets. The pellets were re-dispersed in ethanol with
92 sonication and the centrifugation step was repeated 4 times. The final pellets were dispersed in
93 99% ethanol after filtration (GHP membrane 0.25 μm syringe filters). For nanoparticles containing
94 (3-aminopropyl)triethoxysilane (APS) and N-[3-(trimethoxysilyl)propyl]ethylenediamine (NPD)
95 a small molar amount of APS or NPD (3.3 molar % to TEOS) was added 5 minutes prior to TEOS
96 addition ($_{APS}SiO_2$ and $_{NPD}SiO_2$ particles, respectively). Additional information for preparing other
97 particles, such as liquid phase calcination ($_{CTL}SiO_2$ (T) and $_{CTL}SiO_2$ (Q) particles) and surface
98 functionalization ($_{ASPM}SiO_2$) to tune the dissolution rate, can be found in Supporting Information.
99

100 *Fusarium oxysporum f. sp. niveum (FON) inoculation* FON was isolated from infected watermelon
101 seeds in 2011 and has been stored as monosporic cultures on silica gel at 4 °C. For the current
102 work, potting soil (ProMiX BX (Premier Hort Tech, Quakertown, PA)) was infested with millet
103 inoculum at 0.75 g/L potting soil prior to planting with watermelon seedlings. The detailed
104 preparation on Japanese millet has been described previously.[23] Briefly, autoclaved millet was
105 colonized by FON for 10 days, air dried, and ground in a coffee mill. Watermelon seed*s (Sugar*
106 *Baby)* (Harris Seed Co., Rochester, NY) susceptible to FON were germinated in potting mix and
107 fertilized once 3 weeks after the germination with 40 mL of Peter's soluble 20−10−20 (N−P−K)

108 fertilizer (R. J. Peters Inc., Allentown, PA). When the plants reached the three- to four-leaf stage,
109 seedlings of uniform size of approximately 10 cm height were selected for foliar nanoparticle
110 exposure.
111
112 *Nanoparticle Foliar Application* The concentration of the $_{CTL}SiO_2$ suspension was prepared at
113 1500 mg/L in DI water. It was assumed that this concentration was solely the concentration of
114 SiO_2. Then, the concentrations of the other NP suspensions were adjusted to obtain the SiO_2
115 concentration of 1500 mg/L for each suspension. The adjustment was based on the mass
116 percentage of TEOS added during preparation out of the whole amount of precursor molecules. It
117 was assumed that the calcination didn't affect the amount of SiO_2 within the particles. Additionally,
118 a nonionic surfactant (1 ml/L) (Regulaid®, Kalo Inc., Overland Park, KS) was added to aid
119 dispersion. The suspensions were sonicated for 2 min using a probe sonicator (Fisher Scientific,
120 FB505) to achieve a stable dispersion. The plant was inverted, and the shoot system was immersed
121 into a suspension for 5 seconds to allow for maximum coverage of foliar tissue. Thus, the aerial
122 part of each plant was exposed directly to a SiO_2 suspension of 1500 mg/L. The root part was not
123 exposed to the suspensions. After immersion, the plant was inverted and dried for an hour prior to
124 transplanting for greenhouse growth or field cultivation. Based on a previous research, in which
125 3-4 leaves of tomato seedlings were treated the same way as in this study, in this foliar application
126 each plant sample retains around 1.8 mL of the suspension.[1] Assuming that the watermelon
127 seedlings have comparable size to the tomato seedlings, it was speculated that each plant was
128 exposed to about 2.7 mg of SiO_2 during treatment. Nanoparticle-free control plant was immersed
129 in water containing only the Regulaid surfactant. For the soluble silicate controls, a potassium
130 silicate solution was used (AgSil™ 21, PQ corporation, PA. K_2O : SiO_2 : H_2O = 12.7 % : 26.5% :

131 60.8% by weights) to obtain the SiO_2 concentration of 1500 mg/L in DI water with the surfactant.
132 All silicon treatments were done only one time prior to cultivation.
133
134 *Plant Greenhouse Experiments.* The watermelon seedlings treated with the nanoparticles were
135 then transplanted into pots. Each treatment contained 24 individual plant replicates; 12 plants from
136 each treatment were transplanted into pathogen-free soil and the remaining 12 plants were
137 transferred into media infested with FON. The time-dependent effect of nanoparticles on plant
138 growth/biomass was determined by harvesting three replicate plants from each treatment on a
139 weekly basis for four weeks. For each harvested plant, total wet root and shoot biomass were
140 measured. The experiment was conducted for four weeks.
141
142 *Field Experiments.* Foliar-treated watermelon seedling were transplanted into the field at the
143 CAES Lockwood farm (Hamden, CT). The soil is a Cheshire fine sandy loam (Typic Dystrocrept)
144 (pH 6.1). The field was treated with 10-10-10 NPK fertilizer at the 112 kg/ Ha prior to planting.
145 Plants were set on raised beds mulched with 4 mil black plastic and aligned with drip irrigation
146 tape. Plots/plants were 3.6 m apart. There were ten plant replicates for each nanoparticle treatment
147 or control group; 5 individuals were grown in pathogen-free soil, and the other five plants grown
148 in the plots where 1 g of millet inoculum was thoroughly mixed into the soil at planting. During
149 growth, watermelon fruit were harvested from all plants at 42, 61, and 75 days of cultivation, and
150 the masses of the collected fruits were measured along with the disease progress during cultivation.
151
152 **Results and Discussion**
153 **Silica Nanoparticle Preparation and Characterization**

154 Spherical silica nanoparticles were synthesized via reverse microemulsion. The base particles were
155 prepared only with tetraethylorthosilicate (TEOS), the main silicic acid precursor molecule, and
156 are designated as the control ($_{CTL}SiO_2$). Two different particle types were further prepared by
157 treating $_{CTL}SiO_2$ in organic solvents at high temperatures;100 °C for toluene and 200 °C for
158 squalene: $_{CTL}SiO_2$ (T) and $_{CTL}SiO_2$ (Q). Another two particle types were prepared by incorporating
159 small molar amounts aminosilanes along with TEOS during reverse micro emulsion; $_{APS}SiO_2$: (3-
160 aminopropyl)triethoxysilane (APS), and $_{NPD}SiO_2$: N-[3-(trimethoxysilyl)propyl]ethylenediamine
161 (NPD)). The last particle was similar to $_{APS}SiO_2$, but its surface was functionalized with
162 chlorotrimethylsilane ($_{APSM}SiO_2$). The detailed synthesis route and the characterization is in
163 Supporting Information. Upon foliar application, the nanoparticles could be transferred into the
164 plant through the stomata on the leaf surface. The TEM diameter results (Table 1 and Figure S1)
165 show that only a small population of the $_{APS}SiO_2$ and $_{NPD}SiO_2$ were larger than 100 nm, still clearly
166 nanoscale. Thus, the particles' physical characteristics are similar and all significantly smaller than
167 stomatal openings (typically in the micron range). The zeta potentials of the all particles in Table
168 1 ranged from - 36 mV to - 26 mV; it was assumed that these differences are negligible upon
169 interaction with the much more hydrophobic leaf surface. Overall, the characterization results
170 concluded that the different NPs exhibited equivalent interactions at the leaf surface, which enable
171 the investigation of the effect of dissolution rates on the plant disease resistance ability. During
172 synthesis, TEOS undergoes hydrolysis to form silicic acid ($Si(OH_4)$), and these constituents are
173 polymerized and nucleated to form nanoparticles. The condensation reaction results in the
174 formation of siloxane bonds to form a silica network inside the nanoparticles. When the particles
175 are dispersed in aqueous media after synthesis, the direction of this reaction will be reversed as
176 shown in Scheme 1a. The bond between oxygen and silicon within the silica network is

177 hydrolyzed, and the silicic acid, H_4SiO_4, is released from the particle. This hydrolysis rate can be
178 affected by several parameters such as temperature, pH, ionic strength, and a particle's
179 physical/chemical characteristics.[24,25] For example, in alkaline condition, OH^- nucleophiles can
180 catalyze the bond breaking reaction, and a previous study showed that a more strained silica
181 network can induce a lower activation barrier for hydrolysis.[26] Within the particles, not all TEOS
182 will be hydrolyzed and condensed to form four siloxane bonds per molecule: some molecules have
183 two or three bonds, and the remaining groups will exist as silanol groups. It has been suggested
184 that the rate-determining step for the dissolution kinetic of the silica nanoparticle is the breaking
185 of Si-O bond within the silica network.[27] Thus, in this study it was hypothesized that varying the
186 number of siloxane bond would control the rate of silicic acid release rate from the particles. The
187 slowly dissolving particles ($_{CTL}SiO_2$ (T) and $_{CTL}SiO_2$ (Q)) were obtained via liquid-phase
188 calcination to expedite siloxane bond formation[28] and achieve a higher degree of condensation
189 (Scheme 1b). Conversely, the particles dissolving more rapidly were designed by adding a lower
190 molar amount of aminosilanes (APS or NPD) along with TEOS during synthesis ($_{APS}SiO_2$ and
191 $_{NPD}SiO_2$). APS and NPD were chosen for two reasons. First, it was hypothesized that the
192 propylamine groups and ethylenediamine groups would remain within the particles, lowering the
193 overall degree of condensation as the groups cannot be hydrolyzed and condensed to form siloxane
194 bonds (Scheme 1c). Second, it is known that in aqueous media, the primary amine groups can
195 catalyze the hydrolysis reaction of siloxane bonds.[29–31] Thus, it was expected that the synergistic
196 effects from the low condensation degree and catalytic hydrolysis would result in more rapid
197 particle dissolution. An additional strategy to delay the hydrolysis of the particles will be discussed
198 later and involves chlorotrimethylsilane (TMS) condensation on the APS-containing particles
199 (Scheme 1d, $_{APSM}SiO_2$).

200

201 **Table 1.** Various physical/chemical properties of SiO_2 nanoparticles

	Hydrodynamic diameters (nm) [a]	Zeta potentials (mV) [a]	TEM diameters (nm)[a]	Surface area (m^2/g)
$_{APS}SiO_2$	97.5 ± 0.5	- 23 ± 1	56 ± 16	51.3
$_{NPD}SiO_2$	145 ± 3	- 38 ± 1	57 ± 36	59.8
$_{CTL}SiO_2$	74.9 ± 0.4	- 35 ± 2	53 ± 8	64.2
$_{CTL}SiO_2$ (T)	93.2 ± 0.8	- 28 ± 3	49 ± 8	65.0
$_{CTL}SiO_2$ (Q)	109.8 ± 0.9	- 36 ± 2	51 ± 11	64.0
$_{APSM}SiO_2$	118 ± 2	- 36 ± 2	57 ± 24	54.5

202 [a]The errors in the hydrodynamic diameters, zeta potentials, and TEM diameters represent the
203 standard deviation.

204

205 **Scheme 1**. Schematic descriptions of the silica networks in different silica nanoparticles. (a)
206 General hydrolysis, condensation, and siloxane bond formation within silica. (b) Liquid-phase
207 calcination for enhanced condensation. (c) Condensed APS (left) and NPD (right) silanes in silica
208 nanoparticles. (d) The hydrophobic modification on silica nanoparticle surfaces.

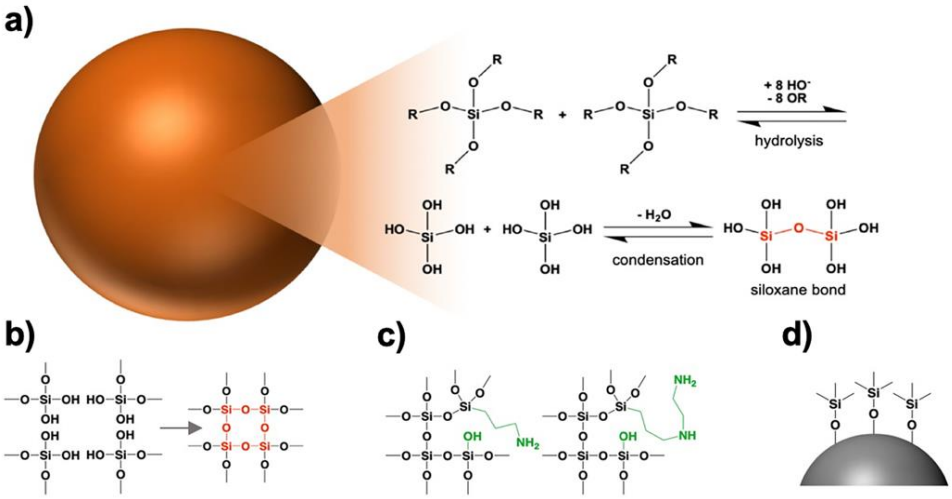

Dissolution Rates of the Silica Nanoparticles

As described previously, it was speculated that the aminosilane-containing nanoparticles would degrade more rapidly than the other nanoparticle types. To investigate it, their physical changes during incubation were compared to aminosilane-free particles. In distilled pure water, $_{CTL}SiO_2$ and $_{APS}SiO_2$ were dispersed and their morphology and density changes were measured every 8 hours (Figure 1a and b). It was obvious that, compared to a small degree of density change at $_{CTL}SiO_2$, $_{APS}SiO_2$ showed a much more aggressive change, including the formation of hollow structures after only 8 hours. These results indicate active hydrolysis in the inner regions, particularly for the larger silica. However, further incubation did not induce complete dissolution of the particles: the shell of the $_{APS}SiO_2$ nanoparticle remained intact even after 2 months of incubation (data not shown).

Given the high hydrophobicity of the plant leaf surface, it was expected that the nanoparticles' surface chemical hydrophilicity or hydrophobicity would be as important as size with regard to reactions at the plant biointerface. The zeta potential values in Table 1 indicate that all particles are negatively charged, regardless of the presence of the aminosilanes and the small amounts of

226 chlorotrimethylsilane on the surface. This is particularly important as it implies that the majority
227 of the aminosilanes are located and condensed inside the particles, making the surface chemical
228 properties consistent across all particle types. Nitrogen adsorption-desorption measurements
229 confirm that all particles lack meso-porosity and are nearly non-porous structures with very similar
230 surface areas. The dissolution rates of each particle were further observed by the silicomolybdic
231 acid (SMA) spectrophotometric assay to quantify monomeric or oligomeric silicic acids released
232 from the nanoparticles.[32] The concentration of the silicic acids was measured every five days for
233 a month upon incubation in simulated xylem sap.[23] Simulated xylem sap was used as a simplified
234 model of natural xylem sap, an interior fluid in plants. As shown in the Figure 1c inset, the initial
235 silicic acid concentration found from the five suspensions was equivalent, indicating that there was
236 no significant difference in the amounts of dissolved silicic acids from all particles during the
237 suspension preparation. However, after five days, the $_{APS}SiO_2$ and $_{NPD}SiO_2$ reached their
238 equilibrium state in terms of hydrolysis, whereas $_{CTL}SiO_2$, $_{CTL}SiO_2$ (T), and $_{CTL}SiO_2$ (Q) released
239 only 46.6, 32.5, and 14.2 % of their silicic acid, respectively. $_{APS}SiO_2$ showed a slightly faster
240 dissolution rate than $_{NPD}SiO_2$ during first five days (data not shown). The remaining three particles,
241 $_{CTL}SiO_2$, $_{CTL}SiO_2$ (T), and $_{CTL}SiO_2$ (Q), continuously dissolved over the incubation period. It was
242 noted that four of the particles ($_{APS}SiO_2$, $_{NPD}SiO_2$, $_{CTL}SiO_2$, and $_{CTL}SiO_2$ (T)) released nearly
243 equivalent amounts of silicic acid to the media by the end of the incubation, confirming that the
244 dissolution behaviors of the particles can be controlled with the same total amount of released
245 silicic acid amount in the end. This consistency is particularly important for agricultural
246 applications given that having different total amounts delivered would be problematic and
247 confound use. As evident after one month of incubation, the silicic acid concentration from $_{CTL}SiO_2$
248 (Q) was still far lower. As such, $_{CTL}SiO_2$ (Q) was excluded from the plant application studies and

as an alternative, the surface of the $_{APS}SiO_2$ was modified with a small amount of the hydrophobic silane TMS (Scheme 1d). It was expected that this modification would delay water access to the nanoparticle surface to slow hydrolysis and dissolution. In fact, as shown in Figure S2, $_{APSM}SiO_2$ showed a delayed silicic acid release relative to $_{CTL}SiO_2$. This new particle type has the same molar amount of aminosilane as $_{APS}SiO_2$, but dissolves more slowly. Thus, the effect of a small amount of nitrogen (or amine group) on the plant, regardless of the particles' dissolution rates, can be monitored as a function of plant responses. The molecular analysis with NMR experiment suggested that the catalytic hydrolysis induced by amine groups in APS and NPD is the main driving force for the faster silicic acid release (See Supporting Information).

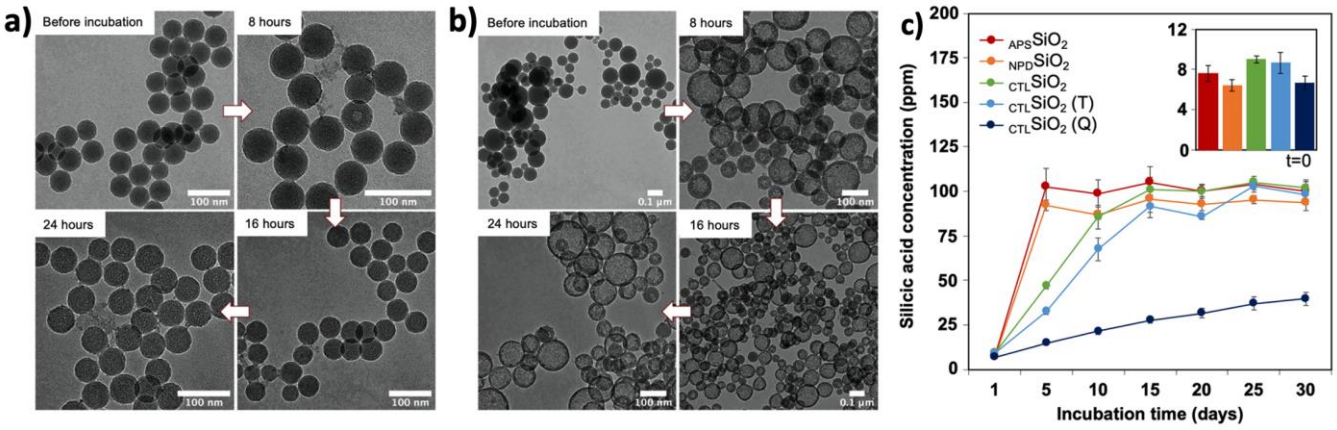

Figure 1. Silica nanoparticle dissolution experiments. TEM images of the nanoparticles, (a) $_{CTL}SiO_2$ and (b) $_{APS}SiO_2$, after incubation in distilled water at room temperature at concentration of 500 mg/L. (c) SMA assay of the silica suspensions in simulated xylem sap. (c) SMA assay of the five silica suspensions in simulated xylem sap at concentrations of 150 mg/L. The inset represents the silicic acid concentrations right after dispersion. The results are the average of three replicate suspensions, and the errors bar represent the standard deviation.

266 **Greenhouse Plant Experiment**

267 Silicon application to the seedlings was conducted via a leaf immersion method (Figure S7).[23]
268 Nanoparticle treatment to the plants were preceded by a silicate salt solution treatment as a control
269 in a separate experiment; here, plant response was equivalent to the untreated healthy/diseased
270 controls, suggesting the need of an alternative application method (Figure 2ab). In the experiment
271 with the particles, the plants applied with nanoparticle once prior to transplanting into FON-
272 infested potting mix or non-infested potting mix were cultivated in a greenhouse. Three replicate
273 plants in each treatment were destructively harvested each week for their biomass measurement;
274 no statistically significant differences were evident among healthy plants as a function of treatment
275 (Figure 2c). This result is not surprising as many studies have reported that silicon-based
276 amendments fail to promote growth in the absence of stress.[18] However, under disease-stressed
277 conditions, plants treated with $_{APS}SiO_2$ and $_{NPD}SiO_2$ showed significantly enhanced biomass
278 compared to the nanoparticle-free plants (Figure 2d). Specifically, compared to the nanoparticle-
279 free plants, $_{APS}SiO_2$-treated plants showed 50.0% increased biomass at week 4; similarly, 74.4%
280 enhanced biomass was observed from $_{NPD}SiO_2$-treated plants at week 2. It is clear that plants
281 treated with other particles ($_{CTL}SiO_2$, $_{CTL}SiO_2$ (T), and $_{APSM}SiO_2$) did not show this growth
282 improvement. Interestingly, these plants and nanoparticle-free plants showed gradual decrease in
283 biomass compared to the values at week 1 as a result of *Fusarium wilt*. However, the biomass of
284 the plants treated with $_{APS}SiO_2$ and $_{NPD}SiO_2$ were maintained or enhanced. Although $_{NPD}SiO_2$-
285 treated plants showed decreased biomass at week 4, we note that after 5 weeks, all plants had died,
286 regardless of particle treatments (not shown here). The watermelon seedlings in greenhouse
287 experiment were grown in small pots with potting soil that was infested with the pathogen. All
288 plants were exposed to the pathogen, and as disease sets in, growth is limited. In addition, under

the growth conditions of this specific experiment, the nutritional source for the plants was rather limited, and the inoculum density of the pathogen was higher than what would be likely in the field. This inoculum load was deliberate so as to ensure uniform infection. As a result, although the plants were metabolically active and attempting to grow, they were unable to accumulate significant biomass. Even in this severe condition, plants treated with $_{APS}SiO_2$ and $_{NPD}SiO_2$ showed improved growth with statistical significance. Even though these plants were not able to maintain improved biomasses due to the severity of the infection, these phenomena were clearly particle treatment-related results, highlighting that particle types with fast silicic acid release were the most effective at stimulating growth in the presence of disease.

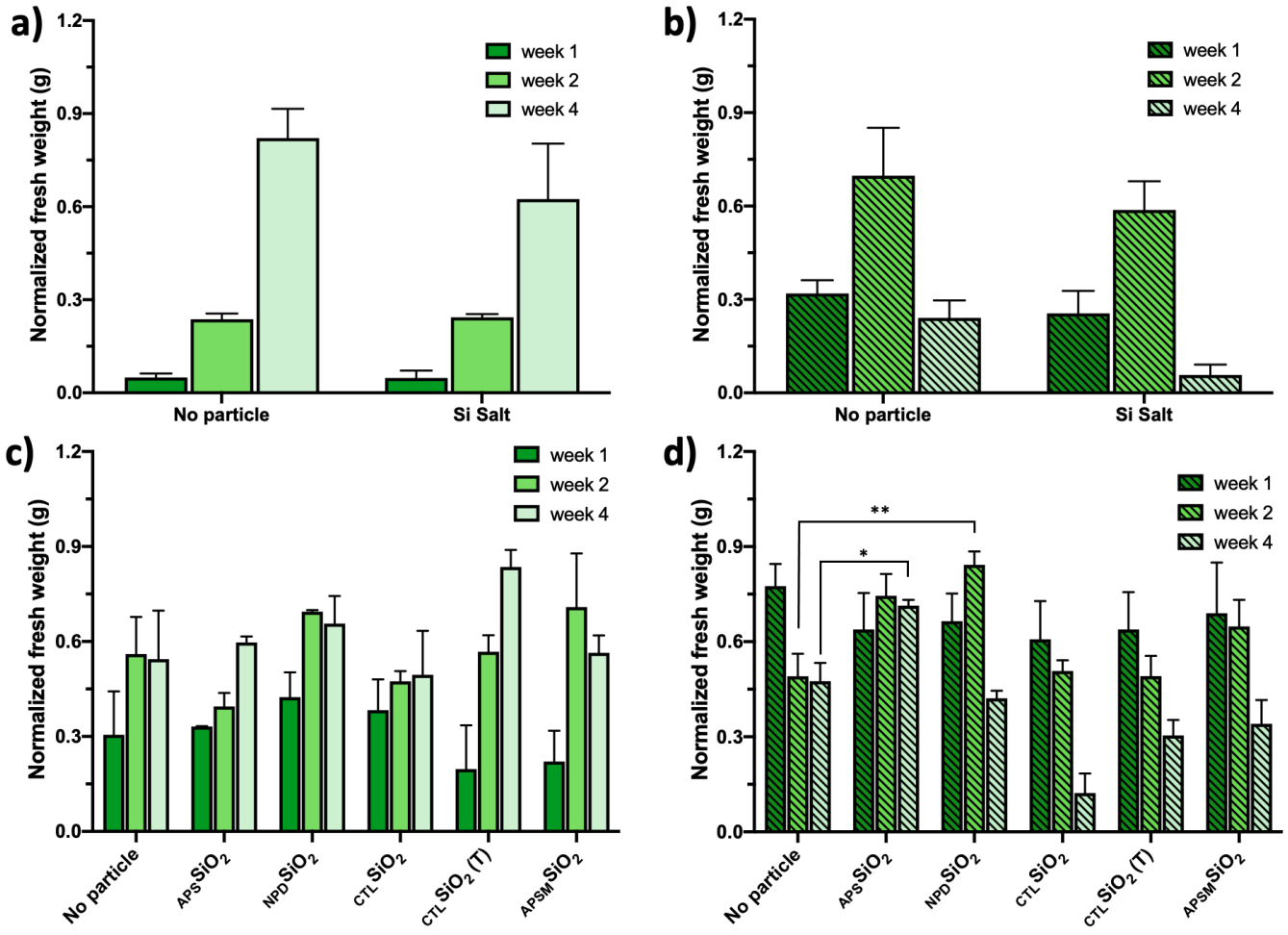

300 **Figure 2**. Biomass of (a,c) healthy and (b,d) Fusarium-infected watermelon seedlings cultivated
301 in the greenhouse for 4 weeks. Each week, 3 replicates of each treatment were harvested, and
302 biomass was measured. The results in each experiment were normalized to compare among
303 treatments. The error bars represent the standard error. The statistical significance testing was
304 performed via a one-way ANOVA with Dunnett's multiple comparisons test to compare effects of
305 the different treatments to the no particle treatments, within a same harvest time point. *$p < 0.05$,
306 **$p < 0.01$.

307

308 **Plant Tissue Elemental Analysis**

309 The elemental content of individual plant tissues was determined across all treatments via ICP-
310 OES. The silicon concentration in the leaves were expectedly higher than the untreated controls,
311 as the detected silicon may include fractions of the element on the leaf surface that have not entered
312 the stoma (Figure S8). Furthermore, all plants treated with the nanoparticles/Si salt showed time-
313 dependent decrease in the concentration of silicon. Although the precise mechanism is unknown,
314 the time-dependent increase in silicon concentration in the leaves of untreated plants under
315 healthy/diseased conditions suggests the migration of Si sources to other tissues through stoma
316 can be a factor which induces the time-dependent decrease in silicon concentration for the plants
317 treated with silicon.

318 The ICP-OES analysis of root tissues (Figure 3) showed that all plants, regardless of the Si
319 treatment, in both healthy/diseased conditions had time-dependent increase in silicon
320 concentration; this differs from the above-ground tissue. This suggests that during the 4 weeks of
321 cultivation, the root tissues absorbed silicon from soil. Interestingly, only plants treated with the
322 rapid dissolution particles ($_{APS}SiO_2$ and $_{NPD}SiO_2$) had significantly greater silicon concentrations

323 than untreated plants. Given that all plants were cultivated in the same media, differences in silicon
324 content can be directly related to the growth and metabolism of the root tissue as a function of
325 treatment. Thus, additional elements (Ca, Zn, and Mn) were investigated for the plants treated with
326 the nanoparticles; however, no relationship was evident between the type of the applied
327 nanoparticles and the content of these nutrients (Figure S9, S10, and S11). Furthermore, the
328 amounts of the five nanoparticles absorbed through stomata shouldn't be different, as the particle
329 sizes are uniform and very similar. Thus, all plants were treated with the same mass dosage of SiO_2
330 prior to cultivation, and the root Si concentration variation is likely to be caused by the amount of
331 silicic acid available from each particle, which directly related to the dissolution rates of the
332 particles. The increased silicon concentrations from the plants treated with $_{APS}SiO_2$ or $_{NPD}SiO_2$ are
333 clearly from the dissolved silicic acids as those two nanoparticles dissolve much more rapidly than
334 the other nanoparticles, and all plants were treated with the same mass dosage of SiO_2 prior to
335 cultivation. To prove the same dosage of silicon across the particle types, in Figure S12, the mass
336 percentages of silicon in each infested plant sample harvested each week are presented.
337 Interestingly, there were some modest differences in Si content across the different nanoparticle
338 types, although there appear to be no consistent trends or patterns. Furthermore, each plant
339 (biological replicate) should have its own silicon amount which should vary among plants and
340 each plant should have its own biological metabolism, which would be hard to distinguish.
341 However, it seems obvious, from much higher Si mass percentages of the nanoparticle-treated
342 plants than the control plants, that the nanoparticle uptake is a major driving force inducing a high
343 Si mass percentage, up to above 0.04%. Based on these outcomes, Figure S12a clearly shows that
344 different nanoparticle treatments didn't result in varied uptake by the plants, indicating that all
345 nanoparticles interact with the plants in a similar way upon the foliar application. Figure S12b

346 shows the Si mass percentage for the plants treated with Si salt solution, which showed no
347 difference from the control, proving that Si treatment in the nanomaterial form can be a more
348 efficient delivery strategy. In addition, to investigating the effect from NP treatment with the
349 improved weight during greenhouse experiments, the correlations between Si concentration in root
350 and shoot induced by NPs and the fresh weights were measured in Figure S13 and Figure S14.
351 Generally, due to limitations in plant experiments where unknown mechanisms and inherent
352 biological variability are present, the coefficient of determination values obtained were below 0.65.
353 However, some important trends were found. First, the infested plant samples showed stronger
354 correlation than the plants in healthy condition. This trend implies that the effect of silicon
355 treatment stands out more when the plants is under infection. Furthermore, both in shoot and root,
356 as time went by, the correlation becomes clearer, especially at week 4. As shown in Figure S8, the
357 measured silicon concentration in shoots decreased when the plants were treated with particles.
358 This occurred because the ICP measurement, especially in early cultivation periods, was likely to
359 involve the particle on the surface of the shoot. These adsorbed nanoparticles should decrease
360 during cultivation, and this was observed via ICP measurement. Thus, in week 4 the concentration
361 of Si in shoot should involve a higher percentage of the nanoparticles or dissolved silicon inside
362 the plants than the previous weeks, and the correlation in week 4 in Figure S13 between the silicon
363 concentration and the fresh weight was much closer than the other weeks, proving the effect of NP
364 treatment. Even though the correlation is weak, the same trend was observed in the root (Figure
365 S14). The investigation of the gene expression levels for the same plant samples was also
366 conducted (see Supporting Information, Figure S16), but no clear correlation between the
367 dissolution rates of the particles and the expression levels of the related genes were found. Given
368 this and the results from elemental analysis, it can be inferred that the enhanced disease resistance

369 ability from the plants treated with fast dissolving particles may have been caused by improved
370 physical barrier formation: the higher amounts of silicon accumulated in the root parts resulted in
371 a more effective prevention of the fungi penetration from the soil to the plants. Importantly, this
372 was a nanoscale-specific phenomenon. Compared to the traditional method, where most of the
373 nutritional sources are absorbed through the root contacting soil, the foliar application method can
374 avoid nutrient fixation, be less affected by soil condition, and provide the plants with nutrients
375 more directly.[33] From the biomass and elemental analysis results, it can be argued that the
376 nanoparticles have some advantages over silicate solution form in terms of delivery. In foliar
377 application, the stomata should be a main route through which the nutrients can access. Due to the
378 high hydrophilicity of the silicic acid dissolved in water, the efficiency might be highly limited in
379 hydrophobic leaf surface. Compared to the silicic acid in solution, the nanoparticles can be
380 transferred to the plant media more efficiently through the stomata as a single nanoparticle can
381 carry a large amount of silicic acid as well as the weight of the nanoparticles can promote the
382 absorption.
383
384

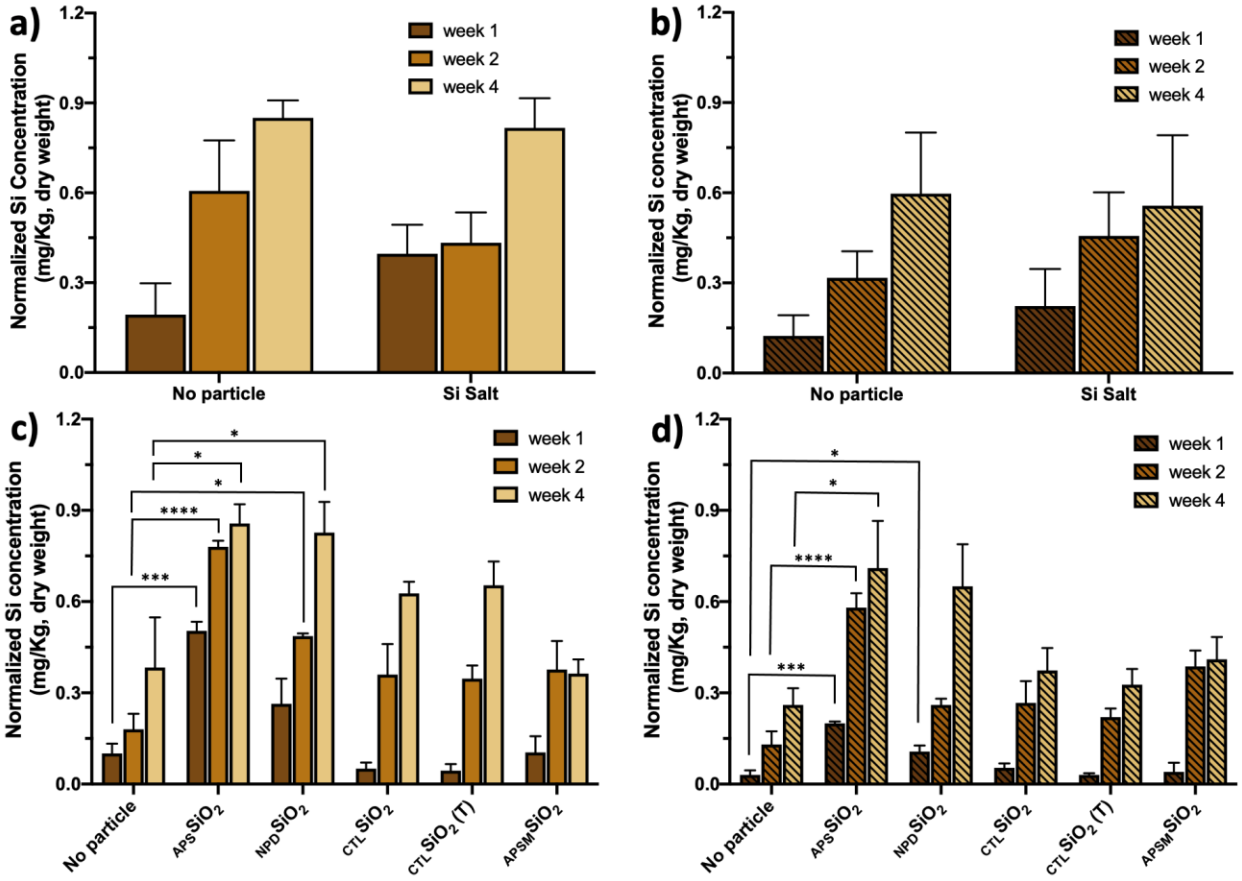

Figure 3. Root Si content of (a,c) healthy and (b,d) Fusarium-infected watermelon seedlings cultivated in the greenhouse for 4 weeks. Each week, 3 replicates of each treatment were harvested, and the root tissues were separated and prepared for ICP-OES analysis. The results in each experiment were normalized to compare among treatments. The error bars represent the standard error. The statistical significance testing was performed via a one-way ANOVA with Dunnett's multiple comparisons test to compare effects of the different treatments to the no particle treatments, within a same harvest time point. *$p < 0.05$, ***$p < 0.001$, ****$p < 0.0001$.

Field Plant Experiment

395 Based on success in the greenhouse, a similar experimental design was used in a field study
396 where plants were grown to obtain marketable fruit yield. Estimates of cumulative disease progress
397 presented as the area-under-the-disease-progress curve (AUDPC) were taken; the lower values
398 indicate less disease presence (see Supporting Information for the detail). All plants grown in non-
399 infested field soils were healthy and showed consistent cumulative AUDPC values without any
400 differences among the nanoscale Si and the untreated controls (Figure 4a). However, plants grown
401 in infested soil developed typical symptoms of Fusarium wilt. The plants that received silica
402 nanoparticle treatments as seedlings exhibited lower mean cumulative AUDPC values than those
403 of the untreated disease control plants, suggesting that silica nanoparticle treatment at the seedling
404 stage effectively suppressed Fusarium wilt in full life-cycle grown plants in the field (Figure 4b).
405 It is also clear that as the particle type dissolution rate decreased, the prevalence of disease
406 increased: Specifically, plants treated with $_{APS}SiO_2$ and $_{NPD}SiO_2$ showed 48.1 % and 37.3 % lower
407 AUDPC values, respectively, when compared to the untreated diseased plants with statistical
408 significance (Figure S15a). Although the other particles were statistically equivalent to the infected
409 untreated controls, the trend for the measured AUDPC followed the same pattern of dissolution
410 observed in the laboratory; the slower the release, the greater the observed disease. This
411 relationship may also explain the differences in fruit yield (Figure 4cd). Similar to the greenhouse
412 experiments, fruit yield in non-infested microplots was unaffected by treatment. However, for
413 diseased plants, nanoscale Si amendment resulted in increased crop yield with a larger number of
414 fruits and masses. Plants treated with $_{APS}SiO_2$ yielded 81.5% more marketable fruit than the
415 untreated controls (Figure S15b). Although large replicate variability confounded statistical
416 analysis, the relationship between the dissolution rates of the particles and the product yield in the
417 data are notable given the single nanoscale application to seedlings 2.5 months prior to harvest.

418 Furthermore, the trends in the data reinforce the contention that the fast-dissolving particles more

419 rapidly delivers silicic acid and conveys benefit under disease-stress conditions.

420

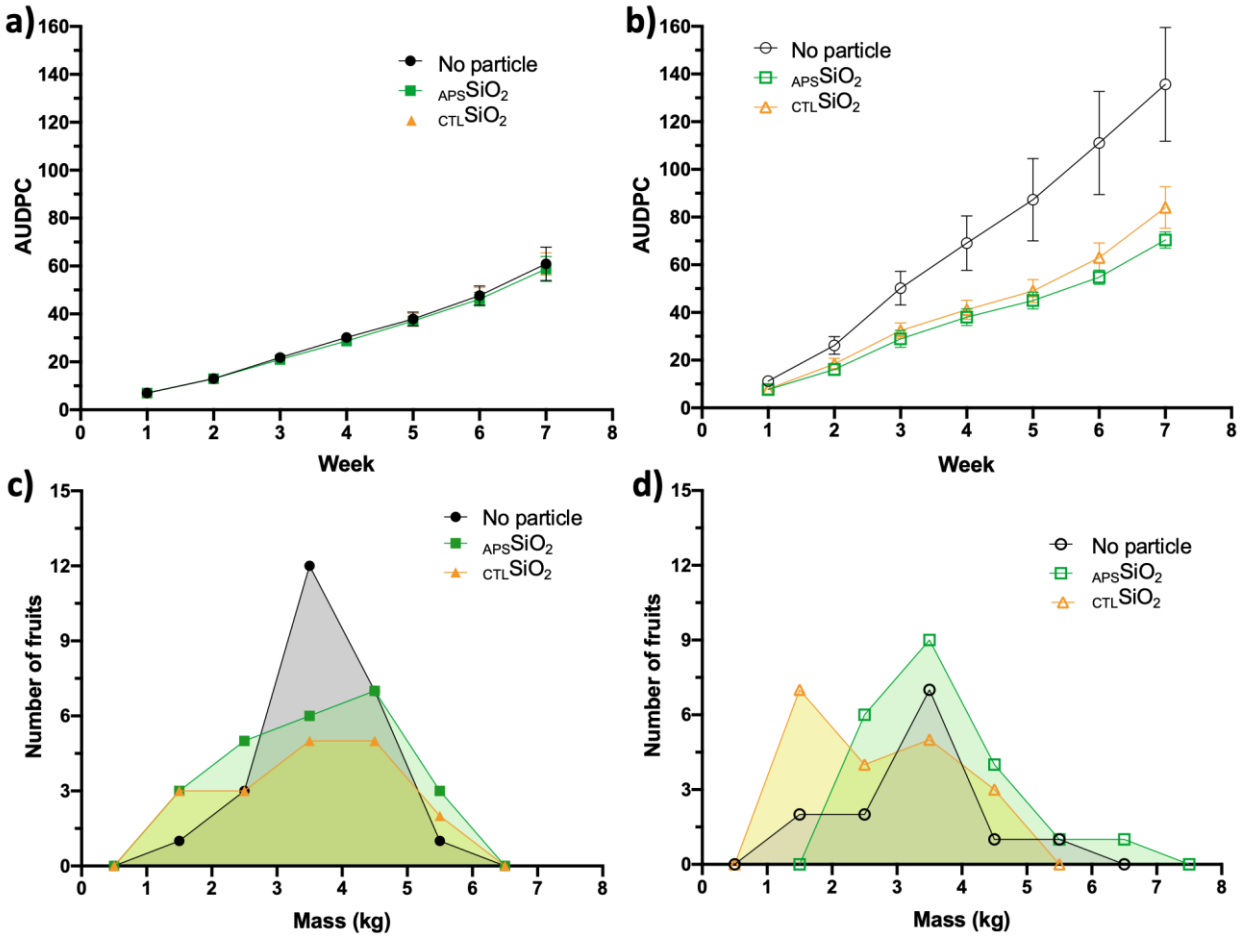

421

422 **Figure 4**. Nanoparticle-treated watermelon plants cultivated in field. AUDPC of the watermelon

423 plants in (a) heathy and (b) Fusarium wilt infected conditions with two representative nanoparticle

424 treatments ($_{APS}SiO_2$ and $_{CTL}SiO_2$) and no particle treatment. Each sample condition had 5

425 replicates, and each week the cumulative disease progress was measured. The error bars represent

426 the standard error. The harvested fruit production yields from the same (c) healthy and (d)

427 Fusarium-infected plants with two representative nanoparticle treatments ($_{APS}SiO_2$ and $_{CTL}SiO_2$)

428 and no particle treatment. The fruits were harvested three times during cultivation, and the results

429 were plotted as a number of fruits corresponding to each mass range (0-1 kg, 1-2 kg, 2-3 kg, 3-4
430 kg, 4-5 kg, 5-6 kg, and 6-7 kg). The AUDPC and the fruit production yields from all 5 different
431 particle treatments can be found in Supporting Information (Figure S15).

432

433 The responses from the plants upon the nanoparticle treatment can be summarized. All
434 greenhouse and field plant-nanoparticle interaction results suggest that the rapid delivery of silicic
435 acids in the form of nanoparticles can be considered highly promising method to enhance the plant
436 disease protection. The positive effects induced by the rapidly dissolving particles clearly
437 demonstrate the importance of providing a silicon source early in the infection process. When the
438 ICP-OES results and gene expression results are combined, it is suggested that the initial supply
439 of silicic acid is critical for enhancing disease resistance of plants by additional silicon deposition
440 reinforcing the cell wall integrity and effectively limited fungal penetration.[34] It is also likely that
441 the presence of additional silicon stimulated innate plant defense systems and secondary metabolic
442 pathways that minimized fungal infection.[35,36] In one recent study, contribution of applied silicon
443 to promote plant hormone salicylic acid , responsible for the activation of pathogenesis-related
444 genes was introduced.[37] However, this phenomenon was not observed from the gene expression
445 experiment. Additional studies are needed to determine the precise mechanisms by which foliar
446 silica nanoparticles with specific surface chemistry enable increased disease tolerance, increased
447 biomass, and greater yield. The goal of the fertilizer is to deliver the desired sources to the plants
448 in efficient way. This study shows that in foliar application, in which the nutrients can be directly
449 absorbed to the plants, the materials in nanoscale form can be beneficial, as well as their dissolution
450 rates can be tuned to maximize their functionality.

451

Supporting Information

The supporting information is available free of charge: Materials and methods for silica nanoparticle synthesis, measuring disease progress, and gene expression analysis; Nanoparticle characterization data; Solid state NMR analysis; Greenhouse experimental details; Field experimental details; Gene expression analysis.

Acknowledgements

This material is based upon work supported by the National Science Foundation under Grant No. CHE-2001611, the NSF Center for Sustainable Nanotechnology (CSN). The CSN is part of the Centers for Chemical Innovation Program. Parts of this work, especially TEM characterization, were carried out in the Characterization Facility at the University of Minnesota, which receives partial support from NSF through the MRSEC program (DMR-1420013). ICP-OES and molecular work done by NZM and CM was supported by USDA NIFA CONH00147 and FDA 1U18FD005505. We acknowledge support from Dr. Alejandro Vidal and Dr. Carla Maria Vidaurre Agut for performing the solid state ^{29}Si MAS-NMR measurements.

Reference

(1) Mueller, N. D.; Gerber, J. S.; Johnston, M.; Ray, D. K.; Ramankutty, N.; Foley, J. A. Closing Yield Gaps through Nutrient and Water Management. *Nature* **2012**, *490* (7419), 254–257.

(2) Lobell, D. B.; Schlenker, W.; Costa-Roberts, J. Climate Trends and Global Crop Production Since 1980. *Science* **2011**, *333* (6042), 616–620.

473 (3) Rodrigues, S. M.; Demokritou, P.; Dokoozlian, N.; Hendren, C. O.; Karn, B.; Mauter, M.
474 S.; Sadik, O. A.; Safarpour, M.; Unrine, J. M.; Viers, J.; Welle, P.; White, J. C.; Wiesner,
475 M. R.; Lowry, G. V. Nanotechnology for Sustainable Food Production: Promising
476 Opportunities and Scientific Challenges. *Environ. Sci.: Nano* **2017**, *4* (4), 767–781.
477 (4) Godfray, H. C. J.; Mason-D'Croz, D.; Robinson, S. Food System Consequences of a Fungal
478 Disease Epidemic in a Major Crop. *Phil. Trans. R. Soc. B* **2016**, *371* (1709), 20150467.
479 (5) Gordon, T. R. *Fusarium Oxysporum* and the *Fusarium* Wilt Syndrome. *Annu. Rev.*
480 *Phytopathol.* **2017**, *55* (1), 23–39.
481 (6) Kah, M.; Tufenkji, N.; White, J. C. Nano-Enabled Strategies to Enhance Crop Nutrition and
482 Protection. *Nat. Nanotechnol.* **2019**, *14* (6), 532–540.
483 (7) Elmer, W.; White, J. C. The Future of Nanotechnology in Plant Pathology. *Annu. Rev.*
484 *Phytopathol.* **2018**, *56* (1), 111–133.
485 (8) Sun, D.; Hussain, H. I.; Yi, Z.; Rookes, J. E.; Kong, L.; Cahill, D. M. Mesoporous Silica
486 Nanoparticles Enhance Seedling Growth and Photosynthesis in Wheat and Lupin.
487 *Chemosphere* **2016**, *152*, 81–91.
488 (9) Cui, J.; Liu, T.; Li, F.; Yi, J.; Liu, C.; Yu, H. Silica Nanoparticles Alleviate Cadmium
489 Toxicity in Rice Cells: Mechanisms and Size Effects. *Environmental Pollution* **2017**, *228*,
490 363–369.
491 (10) Bao-shan, L.; shao-qi, D.; Chun-hui, L.; Li-jun, F.; Shu-chun, Q.; Min, Y. Effect of TMS
492 (Nanostructured Silicon Dioxide) on Growth of Changbai Larch Seedlings. *Journal of*
493 *Forestry Research* **2004**, *15* (2), 138–140.
494 (11) Torney, F.; Trewyn, B. G.; Lin, V. S.-Y.; Wang, K. Mesoporous Silica Nanoparticles
495 Deliver DNA and Chemicals into Plants. *Nature Nanotech* **2007**, *2* (5), 295–300.

(12) Slomberg, D. L.; Schoenfisch, M. H. Silica Nanoparticle Phytotoxicity to *Arabidopsis Thaliana*. *Environ. Sci. Technol.* **2012**, 120827122017009.

(13) Jullok, N.; Van Hooghten, R.; Luis, P.; Volodin, A.; Van Haesendonck, C.; Vermant, J.; Van der Bruggen, B. Effect of Silica Nanoparticles in Mixed Matrix Membranes for Pervaporation Dehydration of Acetic Acid Aqueous Solution: Plant-Inspired Dewatering Systems. *Journal of Cleaner Production* **2016**, *112*, 4879–4889.

(14) Ashkavand, P.; Tabari, M.; Zarafshar, M.; Tomášková, I.; Struve, D. Effect of SiO2 Nanoparticles on Drought Resistance in Hawthorn Seedlings. *Forest Research Papers* **2015**, *76* (4), 350–359.

(15) Abdel-Haliem, M. E. F.; Hegazy, H. S.; Hassan, N. S.; Naguib, D. M. Effect of Silica Ions and Nano Silica on Rice Plants under Salinity Stress. *Ecological Engineering* **2017**, *99*, 282–289.

(16) Tripathi, D. K.; Singh, S.; Singh, V. P.; Prasad, S. M.; Dubey, N. K.; Chauhan, D. K. Silicon Nanoparticles More Effectively Alleviated UV-B Stress than Silicon in Wheat (Triticum Aestivum) Seedlings. *Plant Physiology and Biochemistry* **2017**, *110*, 70–81.

(17) Zellner, W.; Datnoff, L. Silicon as a Biostimulant in Agriculture. In *Burleigh Dodds Series in Agricultural Science*; Rouphael, Y., Ed.; Burleigh Dodds Science Publishing, 2020; pp 149–196.

(18) Rastogi, A.; Tripathi, D. K.; Yadav, S.; Chauhan, D. K.; Živčák, M.; Ghorbanpour, M.; El-Sheery, N. I.; Brestic, M. Application of Silicon Nanoparticles in Agriculture. *3 Biotech* **2019**, *9* (3), 90.

(19) Fauteux, F.; RÃmus-Borel, W.; Menzies, J. G.; BÃ©langer, R. R. Silicon and Plant Disease Resistance against Pathogenic Fungi. *FEMS Microbiology Letters* **2005**, *249* (1), 1–6.

(20) Rodrigues, F. Á.; Benhamou, N.; Datnoff, L. E.; Jones, J. B.; Bélanger, R. R. Ultrastructural and Cytochemical Aspects of Silicon-Mediated Rice Blast Resistance. *Phytopathology* **2003**, *93* (5), 535–546.

(21) Samuels, A. L.; Glass, A. D. M.; Ehret, D. L.; Menzies, J. G. Mobility and Deposition of Silicon in Cucumber Plants. *Plant Cell Environ* **1991**, *14* (5), 485–492.

(22) Finnie, K. S.; Bartlett, J. R.; Barbé, C. J. A.; Kong, L. Formation of Silica Nanoparticles in Microemulsions. *Langmuir* **2007**, *23* (6), 3017–3024.

(23) Borgatta, J.; Ma, C.; Hudson-Smith, N.; Elmer, W.; Plaza Pérez, C. D.; De La Torre-Roche, R.; Zuverza-Mena, N.; Haynes, C. L.; White, J. C.; Hamers, R. J. Copper Based Nanomaterials Suppress Root Fungal Disease in Watermelon (*Citrullus Lanatus*): Role of Particle Morphology, Composition and Dissolution Behavior. *ACS Sustainable Chem. Eng.* **2018**, *6* (11), 14847–14856.

(24) Alexander, G. B.; Heston, W. M.; Iler, R. K. The Solubility of Amorphous Silica in Water. *J. Phys. Chem.* **1954**, *58* (6), 453–455.

(25) Paris, J. L.; Colilla, M.; Izquierdo-Barba, I.; Manzano, M.; Vallet-Regí, M. Tuning Mesoporous Silica Dissolution in Physiological Environments: A Review. *J Mater Sci* **2017**, *52* (15), 8761–8771.

(26) Braun, K.; Pochert, A.; Beck, M.; Fiedler, R.; Gruber, J.; Lindén, M. Dissolution Kinetics of Mesoporous Silica Nanoparticles in Different Simulated Body Fluids. *J Sol-Gel Sci Technol* **2016**, *79* (2), 319–327.

(27) Icenhower, J. P.; Dove, P. M. The Dissolution Kinetics of Amorphous Silica into Sodium Chloride Solutions: Effects of Temperature and Ionic Strength. *Geochimica et Cosmochimica Acta* **2000**, *64* (24), 4193–4203.

542 (28) Cauda, V.; Argyo, C.; Piercey, D. G.; Bein, T. "Liquid-Phase Calcination" of Colloidal
543 Mesoporous Silica Nanoparticles in High-Boiling Solvents. *J. Am. Chem. Soc.* **2011**, *133*
544 (17), 6484–6486.
545 (29) Zhu, M.; Lerum, M. Z.; Chen, W. How To Prepare Reproducible, Homogeneous, and
546 Hydrolytically Stable Aminosilane-Derived Layers on Silica. *Langmuir* **2012**, *28* (1), 416–
547 423.
548 (30) Issa, A.; Luyt, A. Kinetics of Alkoxysilanes and Organoalkoxysilanes Polymerization: A
549 Review. *Polymers* **2019**, *11* (3), 537.
550 (31) Cypryk, M.; Apeloig, Y. Mechanism of the Acid-Catalyzed Si−O Bond Cleavage in
551 Siloxanes and Siloxanols. A Theoretical Study. *Organometallics* **2002**, *21* (11), 2165–
552 2175.
553 (32) Coradin, T.; Eglin, D.; Livage, J. The Silicomolybdic Acid Spectrophotometric Method and
554 Its Application to Silicate/Biopolymer Interaction Studies. *Spectroscopy* **2004**, *18* (4),
555 567–576.
556 (33) Alshaal, T.; El-Ramady, H. Foliar Application: From Plant Nutrition to Biofortification.
557 *EBSS* **2017**, *1*, 71-83.
558 (34) Sun, W.; Zhang, J.; Fan, Q.; Xue, G.; Li, Z.; Liang, Y. Silicon-Enhanced Resistance to Rice
559 Blast Is Attributed to Silicon-Mediated Defence Resistance and Its Role as Physical
560 Barrier. *Eur J Plant Pathol* **2010**, *128* (1), 39–49.
561 (35) Brunings, A. M.; Datnoff, L. E.; Ma, J. F.; Mitani, N.; Nagamura, Y.; Rathinasabapathi, B.;
562 Kirst, M. Differential Gene Expression of Rice in Response to Silicon and Rice Blast
563 Fungus *Magnaporthe Oryzae*. *Annals of Applied Biology* **2009**, *155* (2), 161–170.

(36) Cai, K.; Gao, D.; Luo, S.; Zeng, R.; Yang, J.; Zhu, X. Physiological and Cytological Mechanisms of Silicon-Induced Resistance in Rice against Blast Disease. *Physiologia Plantarum* **2008**, *134* (2), 324–333.

(37) El-Shetehy, M.; Moradi, A.; Maceroni, M.; Reinhardt, D.; Petri-Fink, A.; Rothen-Rutishauser, B.; Mauch, F.; Schwab, F. Silica Nanoparticles Enhance Disease Resistance in Arabidopsis Plants. *Nat. Nanotechnol.* **2020**.

Table of Contents

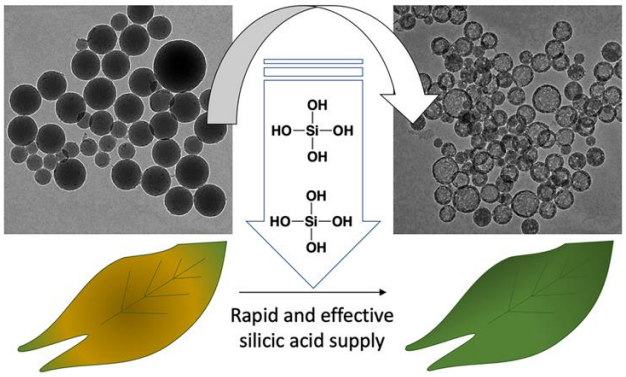

580

581